Slow dynamics process observed in civil engineering structures to detect structural heterogeneities

Philippe Gueguen, Marc-Antoine Brossault, Philippe Roux, Juan Carlos Singaucho

Slow dynamics process observed in civil engineering structures to detect structural heterogeneities

Philippe Guéguen[1], Marc-Antoine Brossault[1], Philippe Roux[1], Juan Carlos Singaucho[2]

1. ISTerre, Université Grenoble Alpes, CNRS, Université Savoir Mont-Blanc, IRD, IFSTTAR, Grenoble, France
2. Instituto Geofisico, Escuela Politécnica Nacional Quito, Ecuador

Corresponding author:
Philippe Guéguen – philippe.gueguen@univ-grenoble-alpes.fr

Abstract

Under strong seismic excitation, the resonance frequencies of civil engineering structures rapidly decrease, followed by slow recovery back to their initial values if there is no damage. In this study, we show that as for laboratory trials with rock samples, the properties of the slow recovery characterize the level of heterogeneities, and in this case, the damage rate. First, we validate this concept with laboratory tests applied to continuous beam-like structures in damaged and undamaged states. One recent model is used to fit the observed recoveries, and we show that its parameters (i.e., frequency variation, recovery slope, characteristic times) change with the health of the equivalent structure. In a second step, this concept is applied to two civil engineering structures that experience earthquakes: the first (Factor Building, USA) without observed damage; and the second (Geophysics Institute building, Ecuador) that experienced a fore/ main/ after-shock sequence with apparent damage that was characterised by a permanent drop in resonance frequency. The efficiency of the proposed model is confirmed for monitoring and for the fit of the frequency recovery. We conclude that the recovery process is a clear proxy of the structural state, and that this could be helpful for seismic monitoring of structural health during earthquake sequences.

Keywords: slow dynamics, recovery, structural health monitoring, earthquakes.

1. Introduction

Elastic waves cause local and reversible disturbances of the medium through which they propagate. This propagation and the time dynamics depend on the elastic properties of the medium. For low-amplitude waves in a homogeneous medium, the behaviour of the material during wave propagation is linear and depends on neither the wave intensity nor the wave shape. On the other hand, non-linear behaviour is classically observed for elastic waves in more complex materials (e.g., granular, heterogeneous), such as rock samples, where the material properties depend on the wave amplitudes. Two types of non-linearity have been described in the literature. 'Classical' non-linearity is generally explained by the consideration of the higher order terms in Hooke's law. However, this theory does not explain some of the observed non-linear phenomena, which are generally known as 'non-classical' non-linearities. In this case, observations refer to both memory effects and hysteresis effects demonstrated by experiments on rock samples (Guyer et al., 1995; Johnson et al., 1996; Guyer and Johnson, 1999). These characterise the dependency of the material response with respect to the stress to which it is subjected, and to its loading history.

After strong dynamic stress, the elastic properties of systems initially deteriorate rapidly, which is followed by a period of slow recovery back to the initial values. Johnson and Sutin (2005) use the terms 'anomalous non-linear fast dynamics' (ANFD) and 'slow dynamics' for these two phases, respectively. There have been many slow dynamics observations on samples: (1) at the laboratory scale (TenCate et al., 2000; Johnson and Sutin, 2005), with the testing of different materials, such as an acoustic probe wave device; (2) at the scale of the Earth crust when subjected to earthquakes (Peng and Ben-Zion, 2006; Brenguier et al., 2008; Wu et al., 2009), by measurements of the regional variations of the wave velocity in the crust next to the faults; and (3) on civil engineering structures (Kohler et al., 2005; Clinton et al., 2006; Guéguen et al., 2016; Astorga et al., 2018), by tracking the resonance frequency of buildings during earthquake sequences. In the acoustic and ultrasonic domains (kHz to MHz), slow dynamics in concrete have been investigated in several studies (e.g., Larose et al., 2013; Shokouhi et al., 2017; Scalerandi et al., 2018). All of these studies reflect the multi-scale invariance of this phenomenon. Both TenCate et al. (2000) and Johnson and Sutin (2005) reported on the non-linear behaviour due to the micro-structure of the materials. They represented this micro-structure as an assembly of grains bound together by contacts and joints. When the material is conditioned by dynamic stress, these contacts and joints can be broken by frictional sliding (i.e., during ANFD), and then they gradually form again at the end of the loading (i.e., during the slow dynamics). These two behavioural phases can be observed and analysed to provide information on the extent of material heterogeneities, and notably the number and size of any cracks present, which is essential information for (although not exclusive to) the definition of the state of health of the material.

In civil engineering, the structure behaviour is characterised by the dynamic response, defined at first order by its modal frequency and damping. During earthquakes, deformation can be significant and can temporarily modify the structural dynamic response (Clinton et al., 2006; Guéguen et al., 2016; Astorga et al., 2018, Zhang et al., 2018). The non-linear response of a structure under dynamic stress is reflected in a rapid variation of its elastic properties, which can be characterized by the variation of its resonance frequencies; this can result in the dynamic opening of cracks in the material. If no damage is observed, these variations are temporary. After a sudden disturbance of its modal parameters, the elastic properties of a structure characterized by its model frequencies slowly recover over time, which includes the closure of opened cracks. The two phases identified by Johnson and Sutin (2005) are thus observed (i.e., ANFD, slow dynamics), as in the laboratory experiments, and they can provide information on the type of heterogeneities present in a structure, and therefore on its structural

health during earthquakes sequence.

The innovative purpose of this study is to examine the ANFD and slow dynamics behaviours of civil engineering type structures at the laboratory scale, and of actual structures under earthquake loading. For the first time, a detailed analysis of the fast and slow dynamics for different state conditions is done, in relation with the structural health. After describing slow dynamics theory in section 2, an initial analysis is carried out in the laboratory on a continuous beam. This is first undamaged and then damaged following dynamic stress similar to that caused by an earthquake. This beam is associated with a structure that shows characteristics and behaviour equivalent to those of a tall civil engineering structure. The same approaches are then applied to two civil engineering structures with permanent instrumentation that suffered major earthquakes: the Factor Building of the University of California–Los Angeles (FB-UCLA; USA) and the Chino Hills earthquake of 29 July, 2008; and the Institute of Geophysics building of the National Polytechnic University in Quito (IG-EPN; Ecuador) and the Pedernales earthquake on 16 April, 2016. In both cases, the ANFD and slow dynamics are analysed and their sensitivity to damage are examined.

2. Theory of resonance frequency recovery

We consider a material characterised by an initial Young's modulus E_0. It is subject to dynamic conditioning that ends at time t_0, which we choose as the origin time $t_0=0$. Recovery of the elastic modulus $E(t>t_0)$ after the loading is a function of time t starting after the end of the stress period. The evolution of the modulus over time during the slow dynamics phase is given by:

$$E(t) = E_0 + \delta E(t) \quad (1).$$

The part of the elastic modulus not yet recovered, $\delta E(t)$, is proportional to the number of contacts that are still broken at time t. The characteristic time τ of the contact formation follows a kinetic law, the Arrhenius equation, which reflects the creation process of barriers of potential energy U at the origin of the grain contacts (Bocquet et al., 1998; Snieder et al., 2016; Shokouhi et al., 2017); i.e.:

$$\tau(U) = \tau_0 e^{U/k_B T} \quad (2).$$

The speed of recovery r of the energy barriers is given by:

$$r(U) = \omega_0 e^{-U/k_B T} \quad (3),$$

where τ_0 is a characteristic time that depends on the material and the type of grains, ω_0 is the corresponding pulsation, k_B is the Boltzmann constant, and T is the temperature. If the initial density of the grain surface without contact is $\rho_0(U)$, immediately after the material conditioning the density at time t can be expressed in the form of an exponential decrease (Tencate et al., 2000); i.e.:

$$\rho_t(U) = \rho_0(U) e^{-r(U)t} \quad (4).$$

The quantity $\delta E(t)$ of Equation (1), which is proportional to the number of contacts that remain broken, is then equal to:

$$\delta E(t) = -A \int_{U_1}^{U_2} \rho_t(U) dU \quad (5),$$

where A is a scale constant and U_1 and U_2 are the lower and upper limits of the potential energy distribution of the barriers in the material. The difference in the elastic modulus at two times t_1 and t_2 can therefore be written as:

$$E(t_2) - E(t_1) = A \int_{U_1}^{U_2} \rho_0(U)\left(e^{-r(U)t_1} - e^{-r(U)t_2}\right) dU \quad (6).$$

As long as the contactless grain surface distribution $\rho_0(U)$ evolves slowly and the times t_1 and t_2 are smaller than the characteristic time τ (Eq. (2)), the difference in elastic modulus between t_1 and t_2 can be approximated by (Tencate et al., 2000):

$$E(t_2) - E(t_1) \approx A\rho_0(U_c)k_B T \int_0^{\infty} (e^{-t_1\tau} - e^{-t_2\tau}) \frac{d\tau}{\tau} \approx A\rho_0(U)k_B T \, ln\left(\frac{t_2}{t_1}\right) \quad (7).$$

This development is based on the established laws of physics (Snieder et al., 2016), and it offers a good explanation for the time dynamics of the logarithmic recovery of the elastic properties of a material after a disturbance (Fig. 1). However, these kinematics are only valid for a limited time period, which excludes the exploration of infinitely short or long times.

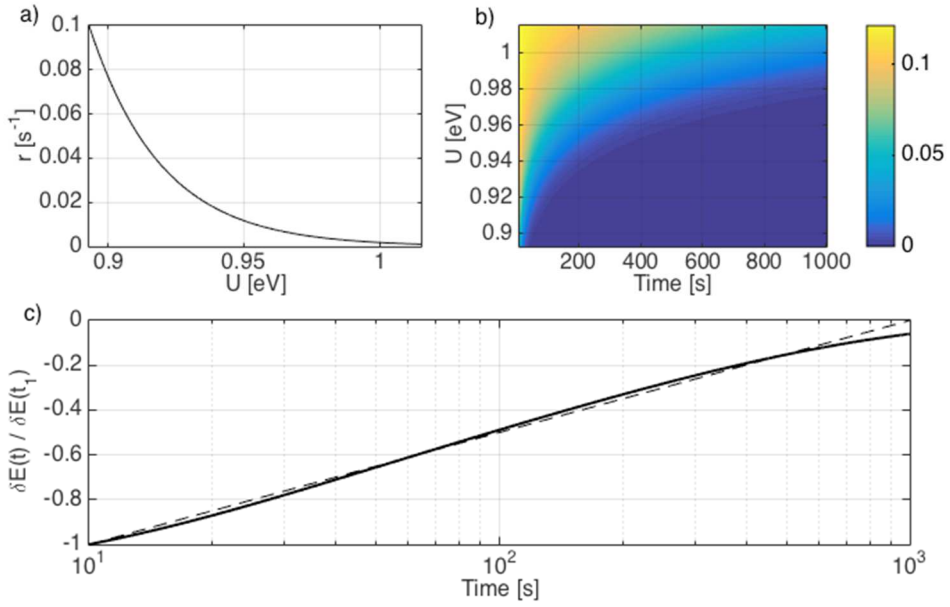

Figure 1. (a) Arrhenius kinetics law for the recovery rate of the energy barriers for the contact of the grains (Eq. (3)). **(b)** Density of the contact surfaces not yet restored (colour scale) as a function of time and activation energy. The initial density is defined as uniform (Eq. (4)). **(c)** Normalized recovery of the Young's modulus calculated through integration of the surface density (Eq. (5)) defined discretely in the time–energy space. The dashed line represents the *log(t)* fit function of the recovery slope.

Snieder et al. (2016) used the basic elements of the aforementioned development by TenCate et al. (2000) to establish a different kinematics law that respects both the logarithmic variation of the recovery for intermediary times and also the flattening at short and long times. Let the time evolution of E(t) of a disturbed system at time t=0 be:

$$E(t) = E_0 + SR(t) \quad (8),$$

where S is a scale constant and $R(t)$ is the function that describes the recovery process, or the slow dynamics. As before, if we assume a superimposition of the processes related to the creation of potential energy barriers U (Eq. (6)) and the corresponding characteristic times τ (Eq. (2)), function $R(t)$ can then be written as:

$$R(t) = \int_{\tau_{min}}^{\tau_{max}} P(\tau) e^{-t/\tau} d\tau \quad (9),$$

where $P(\tau)$ is the density of the state of the relaxation times, and with limits τ_{min} and τ_{max} calculated according to the Arrhenius equation (Eq. (2)):

$$\tau_{min} = \tau_0 e^{U_{min}/k_B T} \text{ and } \tau_{max} = \tau_0 e^{U_{max}/k_B T} \quad (10),$$

where U_{min} and U_{max} are the lower and upper limits of the distribution of contact activation energies in the material. If $N(U)$ is the density of the state of the barriers at the origin of the grain contacts, the number of activation mechanisms where the energy is between U and $U+dU$ is $N(U)dU$. The density of the state $P(\tau)$ can therefore be written as:

$$P(\tau) = N(U) \frac{dU}{d\tau} \quad (11).$$

According to the Arrhenius equation (Eq. (2)), we have:

$$\frac{d\tau(U)}{dU} = \frac{\tau_0}{k_B T} e^{U/k_B T} = \frac{\tau}{k_B T} \quad (12).$$

The substitution of Equation (12) into Equation (11) then gives:

$$P(\tau) = \frac{k_B T}{\tau} N(U) \quad (13).$$

If $N(U)$ remains the same between U_{min} and U_{max}, $N(U)$ is constant. If the temperature T is also constant, the density of the state $P(\tau)$ will be proportional to $\frac{1}{\tau}$. Integrating Equation (13) into Equation (8) gives the model that describes the recovery function by Snieder et al. (2016); i.e.:

$$R(t) = \int_{\tau_{min}}^{\tau_{max}} \frac{1}{\tau} e^{-t/\tau} d\tau \quad (14).$$

This equation cannot be solved analytically. However, unlike the function proposed by Tencate et al. (2000) as a time logarithm, this function converges, regardless of the value of $t \geq 0$, and in particular at short times ($R(0) = \ln\left(\frac{\tau_{max}}{\tau_{min}}\right)$; $R(\infty) = 0$). In the present study, we replace the integration variable τ with $x = t/\tau$, and the time derivative of function R(t) is expressed by:

$$\frac{dR(t)}{dt} = \frac{e^{-x_{min}} - e^{-x_{max}}}{t} \quad (15),$$

where $x_{min} = t/\tau_{min}$ and $x_{max} = t/\tau_{max}$. For $\tau_{min} \ll t \ll \tau_{max}$, which leads to $e^{-x_{min}} \approx 0$

and $e^{-x_{max}} \approx 1$. $\frac{dR(t)}{dt}$ is therefore close to *1/t*, which means that *R(t)* is close to *ln(t)* up to an integration constant. The relaxation is thus expressed as a logarithmic time dependence.

The recovery processes observed in experimental situations can therefore be characterised by different parameters according to Snieder et al. (2016). Snieder et al. (2016) considered the characteristic times τ_{min} and τ_{max}, which characterise the energy involved in the recovery process of contacts of different sizes. τ_{min} and τ_{max} provide more precise information on the type of heterogeneities in the material, and notably on the crack size. They can be calculated from experimental data by measuring the variation of the elasticity modulus or a proxy of this value, such as the resonance frequency of a building in the present study. Here, this corresponds to a non-linear regression adjustment using Equation (14) when the resonance frequency is recovered after the stress. This adjustment and its interpretation according to Snieder et al. (2016) is limited at short times, unless the frequency variations can be measured precisely during and immediately after the stress, and at long times, if the duration of recording is not long enough to observe the full recovery.

3. Data, experiments and data processing

The link between slow dynamics and damage was first verified here at the laboratory scale. In this study, laboratory experiments were carried out on continuous beams. These were not designed to evaluate the invariant scale (i.e., laboratory beam to real-case buildings) of the non-linear behaviour and slow dynamics, but to valid the methods before operational application, as previously done by Brossault et al. (2018). Boutin et al. (2005), Perrault et al., (2013) and Michel and Guéguen (2017) confirmed the analogy to the first order between the response of a tall civil engineering structure and that of a continuous beam. The limestone, beam and experimental set-up used herein (Fig. 2) were described in detail in Brossault et al. (2018). The beam is inserted into the solid limestone base (30 × 30 × 24 cm^3), clamped with epoxy glue, and left free at the top. Its properties are as follows: cross-sectional area, 2 × 5 cm^2; height, 100 cm; density, 2.955 g/cm^3. To measure the horizontal vibrations, two accelerometric sensors are installed (type 4518-003; Brüel and Kjaer), one at the base of the beam, the other at the top. The sensor at the base of the beam is only used to provide an indication of the beam deformation, through calculation of the relative displacement between the top and bottom of the beam during the tests. The data are recorded by a conditioning amplifier (type 2694; Brüel and Kjaer) with an acquisition card (USB-6259; National Instruments).

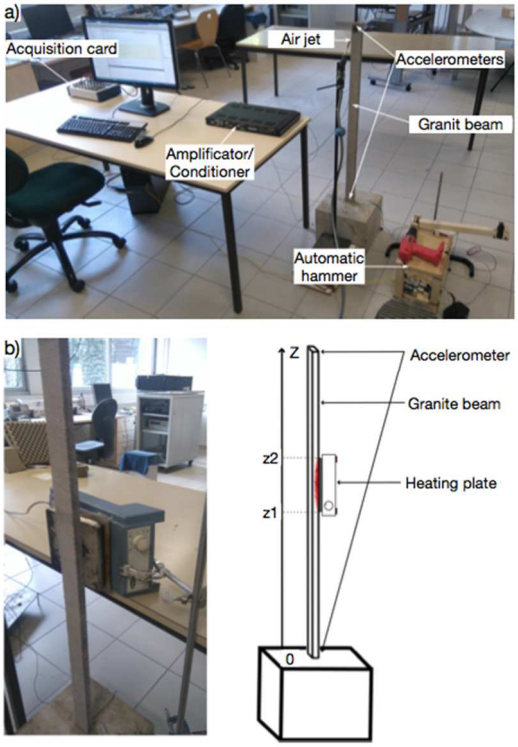

Figure 2. Experimental laboratory device for the granite beam. **(a)** Device for measuring the ambient vibrations generated by the air jet and the automatic hammer. **(b)** Representation of the heating device for damaging the beam, given schematically on the right.

In this study, the beam is subject to continuous stress by an air jet that is applied to the top of the beam. The air jet applies continuous and stationary loading at low amplitude for short times, similar to ambient vibrations recorded in actual structures. Its frequency content is broadband and excites the full range of frequencies considered (1-2,500 Hz). This system was validated by Roux et al. (2014), Guéguen et al. (2014) and Brossault et al. (2018) for continuous measurements of the beam modal parameters. In the laboratory, experimental conditions (i.e., air temperature, humidity, etc.) are constant. Figure 3a illustrates the modal response of the beam obtained herein by Fourier transform of the recording at the top, and is closely comparable to the theoretical frequencies of an analytic model that associates the beam with a free-clamped, Euler-Bernoulli type, bending beam (Brossault et al., 2018).

The resonance frequency variation for the system is monitored over time by the random decrement technique (RDT) (Cole, 1968), which Cole used to construct the impulse response of a system from measured ambient vibrations. Cole (1968) justified this transformation by considering the response of a structure to random loading at time $t+t_0$ as the superimposition of the free response at time t_0 and the forced response to the random loading between t_0 and t. By summing a large number of signal windows with the same initial conditions, the magnitude of the expected random part decreases compared to the magnitude of the impulse response. The result of the summation process is the random decrement signature (*RDS*) expressed thus as:

$$RDS(t) = \frac{1}{N}\sum_{i=1}^{N} s(ti + \tau)|T_0 \qquad (16),$$

where $s(t)$ is the signal, N is the number of windows summed, τ is the duration of the windows, and T_0 is the initial trigger condition (Nasser et al., 2016). When filtered around a mode of the structure, $RDS(t)$ is equivalent to the impulse response of the beam, which then

enables extraction of the modal frequency and damping by adjusting an exponential function. Many studies have provided information on the quality of such an estimate, the processing parameters (e.g., length of windows to be summed, initial conditions) and the restrictions due to the summation process, which has confirmed its effectiveness on actual civil engineering structures (Asmussen, 1997; Mikael et al., 2010; Roux et al., 2014; Nasser et al., 2016). An operational description of the method was provided in Brossault et al. (2018). Although RDT was initially proposed for estimation of damping, the quality, effectiveness and precision of the modal parameter estimation means that we can use it as a time monitoring tool for the frequencies of the granite beam. In the present study, after filtering around the central frequency of the mode (i.e., within ±10% of the modal frequency), we consider the recording lengths of 1000T (T, mode period) and the windows to be summed as 10T (i.e., N = 100 windows), as these processes are considered to offer stable accuracy (Brossault et al., 2018). Figure 3b, c give examples of the frequency time monitoring (mode 3) over 20 h of acquisition and its variability over time, respectively.

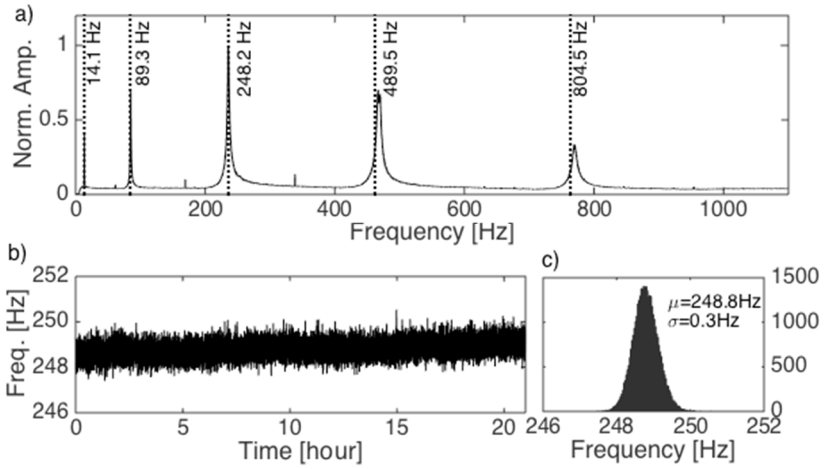

Figure 3. Modal responses of the granite beam. **(a)** Fourier transform from a vibration recording at the top, and comparison (dotted line) with the estimated theoretical modes for the Euler-Bernoulli type continuous beam. Measured values: L × W × H, 2 × 5 × 100 cm; density, 2.69 kg/m^3. Estimated values: Young's modulus, 50 GPa. **(b)** Frequency variation of mode 3 computed over 21 h by the normalized random decrement technique. **(c)** Distribution of the frequencies for mode 3.

The experimental data recorded for the beam subjected to the loading by the air jet are dominated by low-amplitude acceleration ($\approx 10^{-1}\, ms^{-2}$). To load the beam and trigger the slow dynamics, as classically observed in an earthquake sequence, dynamic load is applied to the system in a controlled manner using a programmable automatic hammer that strikes the supporting granite block (Fig. 2a). This enables stable repetition (i.e., of amplitude, duration) of the system conditioning. The effect of the conditioning (or strain level) on the slow dynamic is not analysed in our study. The acceleration generated at the top is $\approx 10^{2}\, ms^{-2}$ and lasts for approximately 5 s. The associated deformation calculated between the top and the bottom of the beam is around 5 ×10^{-5}; i.e., the system remains within the elastic domain. Figure 4 shows mode 3 of the granite beam, calculated as the average of 15 successive impacts. This shows the stable frequency before the impact; then there is a remarkable drop during the impact, as highlighted in red, with fitting of the data with a single logarithmic function of time, as follows:

$$F(t) = A\log_{10}(\mathrm{t}) + \mathrm{B} \quad (17),$$

where *F(t)* is the resonance frequency.

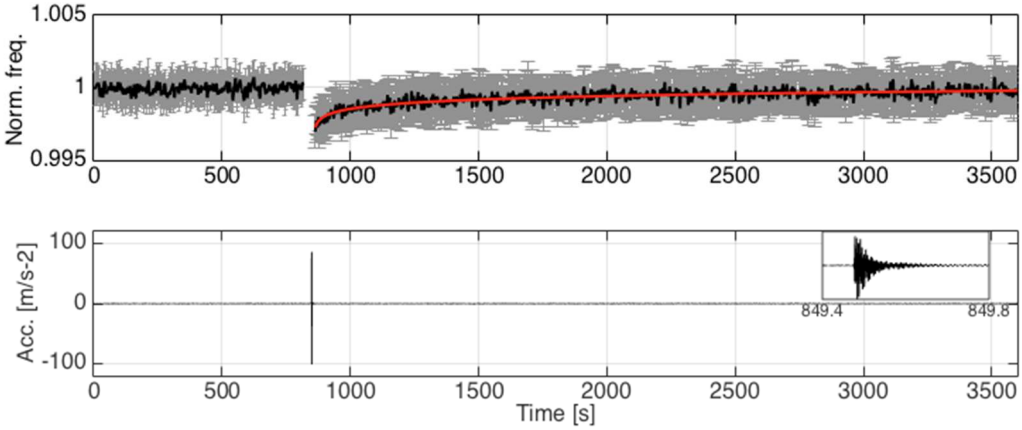

Figure 4. Variation of the frequency (mode 3) during a dynamic solicitation. The red line is the average of 15 repeated trials. The error bars (grey) are the uncertainty of the frequency measurements for the 15 tests. The thick black line is the average. The inset on the right is a zoom of the acceleration during a shock.

It is interesting to note here that the standard deviation of the frequency is constant over time, which indicates the measurement stability for the repetitive hammer strikes at the laboratory scale. The drop in frequency ($\Delta F/F_0$) is around 3.58 $\times 10^{-3}$ for a standard deviation of 10^{-3}.

To evaluate the transitional variations of the resonance frequency and for estimation of the short relaxation times (τ_{min} Eq. (9)), the RDT method was modified to improve the time accuracy, by partially removing the windowing effect for instantaneous frequency variation assessment. The signal stationarity condition justifies the summation of the time windows with the same initial conditions T_0, which means that the estimation would be biased if this condition was not respected. To apply RDT to signal windows that include high amplitudes, use of a normalised RDT (NRDT) is proposed. This consists of normalising each segment before the calculation of the segment average. This normalisation can be considered as a stationarity condition that is imposed artificially on the data, without modifying the amplitude variations within each segment, as an essential condition for signature calculation, and particularly its exponential decrease. Two normalisations were tested: using the maximal amplitude (NRDT1) and the maximal energy (NRDT2) of the time segment.

Figure 5 shows the fundamental frequency variations during an impact from Figure 4 using these three methods, considering a 100T overlap between successive windows. Considering windows of 1,000T, the frequency fluctuations are smoothed, whereas for 400T, there is a significant improvement in the resolution of fluctuations that has a physical meaning, as discussed in Brossault et al. (2018). Monitoring of the transitional variation of frequency at the time of impact is improved, thereby improving the identification of the moment when the recovery begins (i.e., τ_{min}) even if the shift is observed due to the windowing process used for NRDT. The estimation quality is around 4 $\times 10^{-2}$%, which is well below the frequency variation measured during impact. The two normalisation methods are very similar, and only NRDT1 will be used in the rest of the present study.

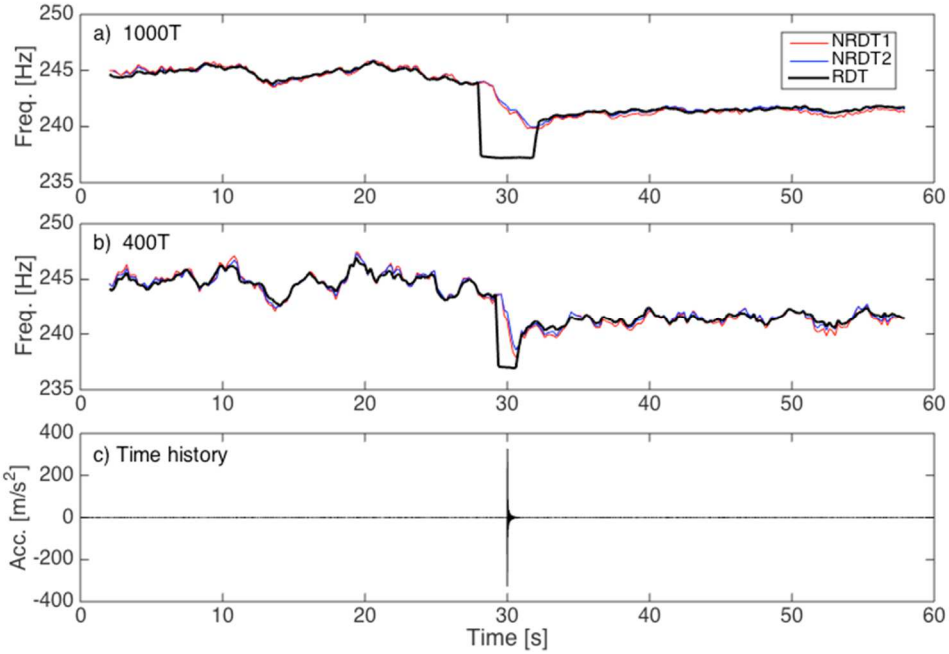

Figure 5. Comparisons of the estimations of the instantaneous frequency variations by the standard RDT method and the NRDT method (cases 1 and 2). **(a)** Window of length 1000T. **(b)** Window of length 400T. **(c)** Time history of the acceleration.

Finally, to define the relevance of the slow dynamics signature to identify damage, the impacts are applied to the beam subjected to the air jet loading before and after application of the damage. Roux et al. (2014) and Guéguen et al. (2014) used moderate local heating of a Plexiglas beam to apply a temporary, localised disturbance. The disturbance proposed herein is also limited in space, but is definitive: a heating plate applied locally (Fig. 2b). This process creates thermal cracks in the granite beam, like in the laboratory tests carried out on granite samples by Chernis and Robertson (1993) and by Takarli and Prince-Agbodjan (2008). The experimental stress represented by the size of the beam and its clamping to the support, as well as the desire to limit the damage to a specific portion of the beam, prevent the use of an oven to heat the sample in a gradual and uniform manner, as was the case in the aforementioned articles. Chernis and Robertson (1993) indicated that the thermal cracking temperature threshold of granite is approximately 80 °C, and that the higher the temperature applied to the granite, the greater the thermal fracturing, and thus the greater the damage characterised by the Young's modulus reduction. Figure 6a shows the effects of heating on the beam, which are characterised by an increase in the acoustic emissions recorded on the beam during the heating, a characteristic of thermal fractures. The consequences to the resonance frequency are shown in Figure 6b. A significant variation is observed after heating: 0.63%, 4.43%, 2.33% and 1.87% for modes 1 to 4, respectively. As shown by Roux et al. (2014), the mode frequency variation is directly dependent on the position of the damage, and the variations between the modes will not be discussed further herein. Only the effectiveness of the damage is relevant to the rest of the present study.

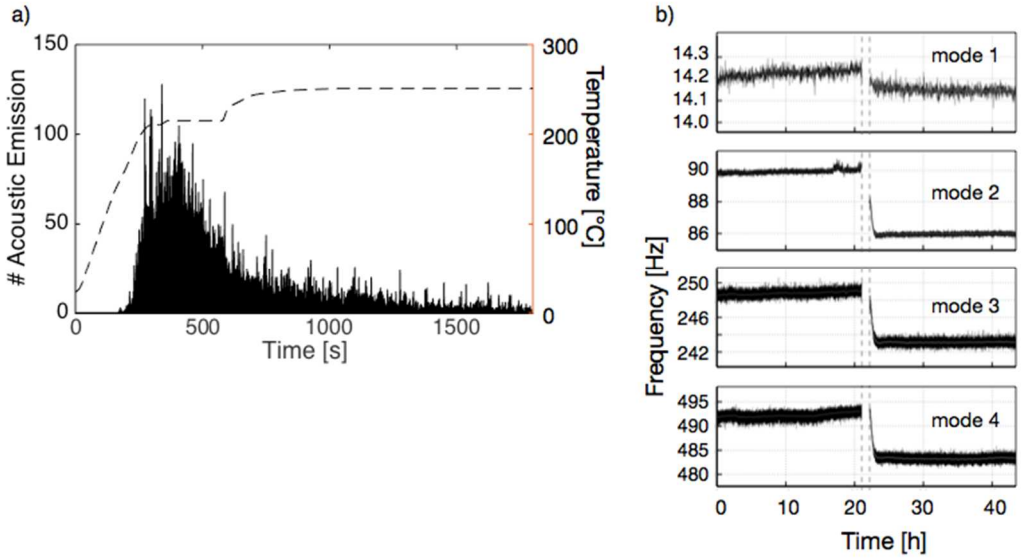

Figure 6. Illustration of the damage by heating to the beam. **(a)** Variation in temperature (dashed line) and number of associated acoustic emissions. **(b)** Variation of the modal (1 to 4) frequencies due to the heating period. Vertical dashed lines indicate heating periods when the modal analysis is interrupted.

4. Analysis of the slow dynamics

The results analysed in this study were obtained from two experiments that comprised a series of 15 impacts that were applied before and after damaging the granite beam. Figure 7 shows the frequency recovery for the first four modes of the granite beam in these two states. Frequency monitoring was obtained by averaging the recovery over the period of the 15 impacts. Figure 7 and Table 1 indicate major modifications of the frequency variation time dynamics after the damage, when all of the modes show a greater frequency drop ($\Delta F/F_0$) associated with an increase in recovery speed (gradient p) for impacts of similar amplitudes. The increase in $\Delta F/F_0$ means that once it has been damaged, the system is less resistant, and reduces its transient stiffness more easily, an observation that was also reported for an actual building during an earthquake (Astorga et al., 2018). $\Delta F/F_0$ and p of the relaxation relationship of Equation (17) ($F(t) = p \log_{10}(t) + (1 - \Delta F/F_0)$ show the same relative increases for the first three modes (and, to a lesser extent, for the fourth mode), which indicates the strong dependency between these two parameters, and ultimately, an identical recovery time specific to the beam, regardless of the mode considered. Nevertheless, Lott et al. (2017, 2018) showed that the strain field controls the non-linear behaviour. Of note, Tencate et al. (2000) normalised the relaxation coefficient p with the strain values of each mode, to consider the sensitivity of the mode to the damage according to its localisation. Indeed, Roux et al. (2014) used the sensitivity of the modal frequencies to the position of damage for localisation, and the strain value of each mode could be considered for normalised p values. In the present study, the strain value is not computed (as only one sensor at the top of the beam was used), although the relation between the strain and the p values of each mode could be used for localisation, following the concept proposed by Roux et al. (2014), but not considered in this study.

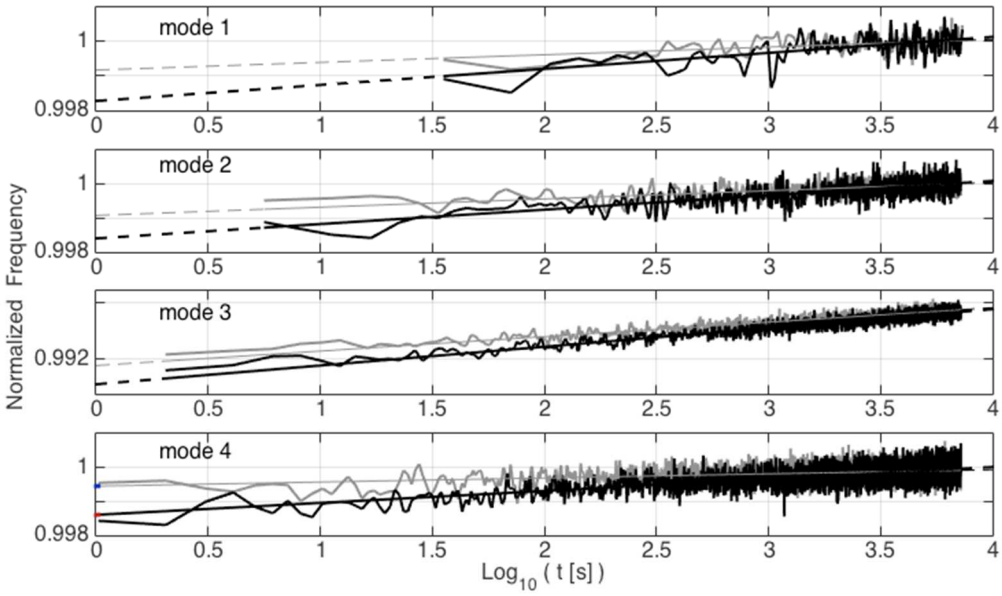

Figure 7. Recovery of the normalised frequencies for modes 1 to 4 of the granite beam before (grey) and after (black) the damage. The recovery is the average of 15 successive shocks. Bold lines: experimental smoothed normalized values of the fundamental frequency; continuous thin lines: linear model fit (Eq. (17)); dotted lines: extension of the model to short times.

Table 1. Values of p and $\Delta F/F_0$ of the recovery relationships of the shape $F(t) = p\log_{10}(t) + (1 - \Delta F/F_0)$ for modes 1 to 4 for an undamaged and a damaged beam. *diff*, variation of the parameter characterising the slow dynamics.

	Mode 1		**Mode 2**		**Mode 3**		**Mode 4**	
	p	**$\Delta F/F_0$**	**p**	**$\Delta F/F_0$**	**p**	**$\Delta F/F_0$**	**p**	**$\Delta F/F_0$**
Undamaged	2.23×10^{-4}	8.25×10^{-4}	2.43×10^{-4}	9.21×10^{-4}	1.26×10^{-3}	5.52×10^{-3}	1.21×10^{-4}	5.48×10^{-4}
Damaged	4.67×10^{-4}	1.73×10^{-3}	4.24×10^{-4}	1.60×10^{-3}	1.64×10^{-3}	7.16×10^{-3}	3.53×10^{-4}	1.40×10^{-3}
diff (%)	109	109	74	74	30	30	192	155

Figure 8 shows the frequency monitoring for mode 3 of the granite beam, as determined by the relaxation model proposed by Snieder et al. (2016) and applied to the experiment results (Eq. (14)). In this example, the frequency monitoring was decimated at the long time logarithmic scale, to reduce the weight of this part in the error calculation used for convergence of the non-linear regression. The frequency drop $\Delta F/F_0$ is initially 4.2×10^{-3} and 5.8×10^{-3} before and after the damage, respectively, for the equivalent conditioning. These values therefore increased by 38.1%, which is the same as the increase observed for this mode when the linear relationship is adjusted according to the time logarithm (30%; Table 1).

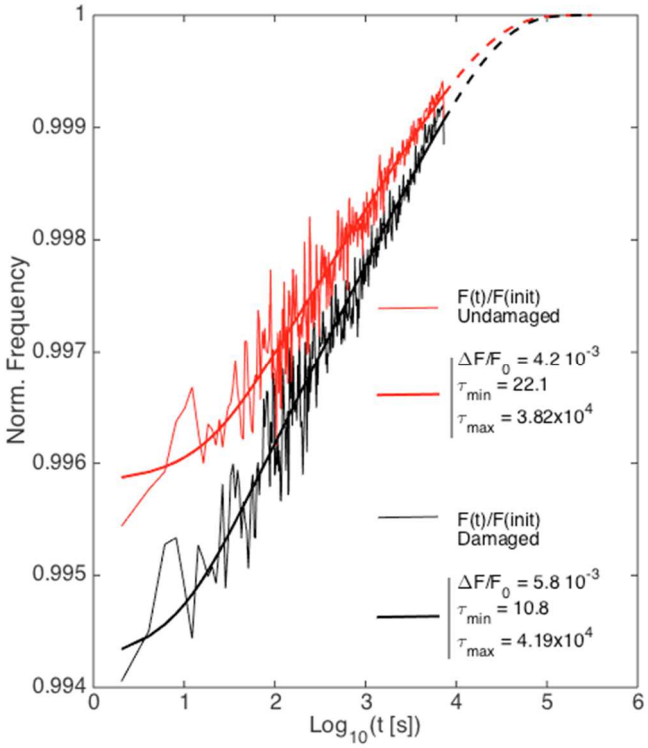

Figure 8. Recovery of the values of the normalised frequencies for mode 3 of the granite beam before (grey) and after (black) the damage. The recovery is the average of 15 successive shocks. Bold lines: experimental smoothed normalised values of the fundamental frequency; continuous thin lines: model fit (Eq. (14)); dotted lines: extension of the model to long times.

Determination of the time constant τ_{max} appears less certain. Indeed, no long-term curvature characterises τ_{max} in the frequency monitoring in either case, with the beam recovery being very slow with respect to the time periods between the repeated impacts. Parameter τ_{min} is determined by the curvature visible for short times; this is 22.1 s for the undamaged beam, and 10.8 s for the damaged beam (Fig. 8). According to Snieder et al. (2016) and the development described in section 1, τ_{min} depends on the smallest characteristic size cracks. Reduction of this constant therefore implies the creation of cracks that are smaller than the heterogeneities initially present in the beam, which is one of the processes that results from damage by heating.

Adjustment of the experiment data of the relaxation relationship proposed by Snieder et al. (2016) provides additional information. The time constant τ_{min} defines the minimal activation energy required to close the cracks in the material, and therefore the smallest characteristic size crack. We can estimate this minimal energy barrier for both states of the beam using the Arrhenius equation, of Equation (2). The energy barrier U is therefore written as:

$$U = k_B T \, log(\tau/\tau_0) \qquad (18).$$

For high temperatures, TenCate et al. (2000) indicated that $\tau_0 \approx \hbar/k_B T$, where $\hbar$ is Planck's constant. The numerical application of Equation (18) gives a minimal energy barrier of 0.829 eV and 0.837 eV for the undamaged and damaged beam, respectively. Thus, there is a moderate reduction in the minimal energy barrier associated with the damage; i.e., the smallest crack size results in a large variation in τ_{min}. This observation is all the more critical

because determining τ_{min} is difficult and depends on the monitoring method used (NRDT in the present case) and the ability to correctly identify the start of the recovery. Longer recovery times are characterised by increasingly small variations, and are polluted by long-term oscillations; e.g., due to temperature fluctuations or successive conditioning.

The fitting of the data with a logarithmic function of time is more robust than the non-linear regression of a complex function, where the parameter determination depends on the first and last measured frequencies. However, the generalised relaxation law in Equation (14) (Snieder et al., 2016) results from the superimposition of characteristic times between τ_{min} and τ_{max} directly proportional to the size (i.e., characteristic time) of cracks. For application to the civil engineering structures, only the Snieder et al. (2016) model will be considered herein.

5. Application of slow dynamics to actual civil engineering structures

The first building considered here is FB-UCLA on the campus of UCLA, which was built in the 1970s. A full description of the structure, the modelling, and the first experimental data were provided in Kohler et al. (2005), Nayeri et al. (2008) and Skolnik et al. (2006). This building has 17 stories, two of which are below ground level. It has a steel structure with brick facing and concrete foundations. Its ground footprint is rectangular, with the long side as the north-south direction. The initial network of 72 accelerometers that was installed in 1994 was upgraded in 2003 by the US Geological Survey, to improve the sensor sensitivity and enable acquisition of ambient vibrations. The present study is focussed on the monitoring of its fundamental mode frequency in the north-south direction, as identified by Kohler et al. (2005) and already monitored using RDT by Guéguen et al. (2016). This mode corresponds to the peak shown on Figure 9 at ~0.6 Hz. The continuous records sampled at 100 Hz that are used in this study come from the station at the top in the south-east corner (station GE, component HNN). The data were downloaded from the IRIS datacentre website (http://www.iris.edu).

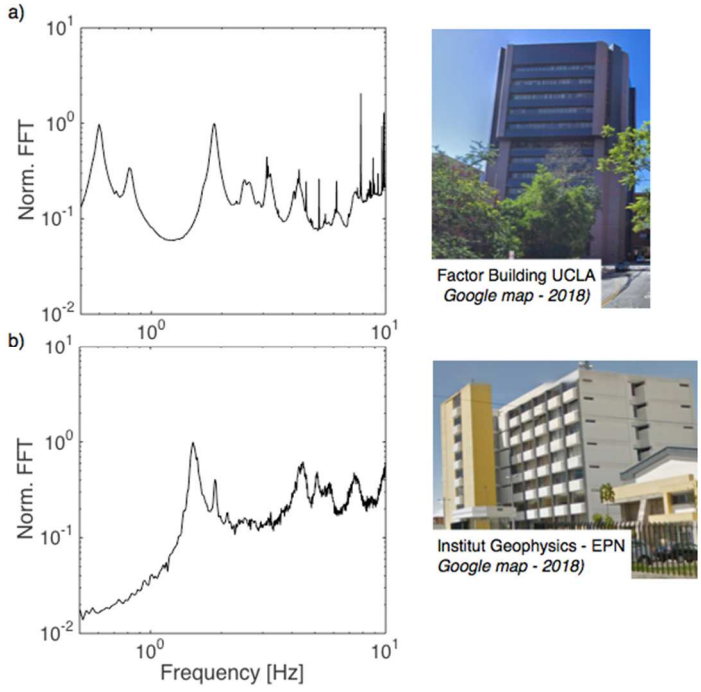

Figure 9. Buildings tested in the present study, and their responses computed as the Fourier transforms of the ambient vibration recording at the top. (a) Factor building (FB-UCLA). (b) Institute of Geophysics (IG-EPN).

The second building used for this study is IG-EPN in Quito, Ecuador, in the National Polytechnic University campus. This was built in 1976 before the first earthquake engineering construction code was introduced in Ecuador. It has eight stories of the same height, each of which comprises a slab supported by reinforced concrete columns. Since 2011, the structure has been permanently equipped with a triaxial accelerometer (GURALP-5TD) positioned at the top. The acceleration is continuously recorded at 100 Hz; this structure shows a resonance frequency of ~ 1.5 Hz (Fig. 9).

For FB-UCLA, the earthquake used is the Chino Hills earthquake of 29 July, 2008, of magnitude 5.5, the epicentre of which was 45 km from Los Angeles. The signal recorded at the top of the structure (Fig. 10) shows an acceleration peak at 1.2 $m.s^{-2}$, and the deformation calculated on the basis of the acceleration indicates a maximal of ~5 $\times 10^{-4}$. For IG-EPN, the 7.8 magnitude Pedernales earthquake on 16 April, 2016, was used, which had an epicentre 170 km from Quito (Fig. 10). The acceleration recorded at the top of IG-EPN during the earthquake shows an acceleration peak of 0.72 $m.s^{-2}$, with the maximal calculated deformation of 7 $\times 10^{-4}$. In both cases, the deformation is below the standard threshold of damage appearance, which is assumed to be ~3 $\times 10^{-3}$.

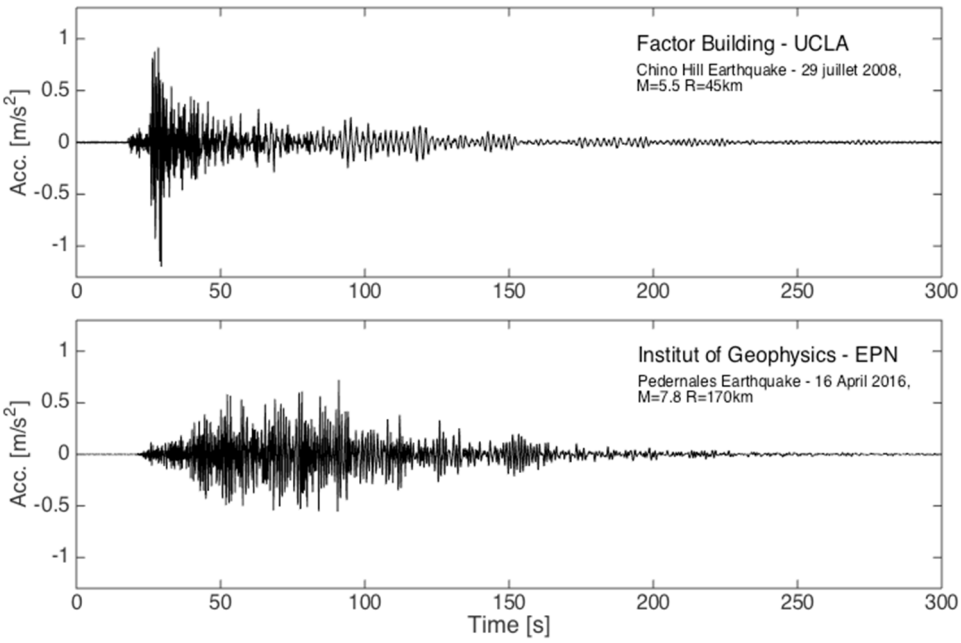

Figure 10. Time history of the acceleration recorded at the top of the buildings for the earthquakes used for the frequency recovery analysis.

The time resolution of NRDT depends on the specific period of the mode of the structure, which is around 1 s for each of these two structures. We used NRDT with the 100T signal duration, after checking the validity of this choice in preliminary tests. The recovery between two successive signal segments is 90%, to reduce the time interval of the monitoring and to enable optimal τ_{min} evaluation. We also chose to validate this by applying a more conventional time–frequency distribution, of the Cohen class. We therefore applied the Wiegner–Ville method that was tested by Michel and Guéguen (2010) on earthquake data recorded for these buildings. The principle is to distribute the signal energy in the time–

frequency space. The energy at a point in the time–frequency space is not calculated in a time window, but between $-\infty$ and $+\infty$. As the signals are finite in time, the distribution actually calculated in practice is therefore the smoothed pseudo Wigner–Ville distribution. This corresponds to the Wigner–Ville distribution for which the energy values of time–frequency pairs are calculated in windows limited in time and in frequency. The frequency range of this distribution is large, which makes it difficult to measure small frequency variations. To counter this difficulty, the reassignment method was applied, as described in Michel and Guéguen (2010). The local energy of the distribution is reassigned to the centre of gravity of the domain around each time–frequency point. Michel and Guéguen (2010) indicated that this reassigned pseudo-distribution is particularly suitable for the measurement of sudden variations in frequency, as for the present case. The value used for the frequency at each time t is then determined by picking the maximum value of the reassigned pseudo Wigner–Ville distribution at that time. Hereafter, we use the term Wigner–Ville distribution (WV) to indicate the reassigned pseudo Wigner–Ville distribution.

Figure 11 shows an example of the monitoring of the fundamental frequency of IG-EPN during the 2016 earthquake, as calculated by NRDT and WV, which characterises the ANFD and slow dynamics. A Savitzky-Golay (Orfanidis, 1995) type of smoothing method is applied to the frequency variations on which the recovery analysis is carried out. The frequency drops by about 30% during the earthquake. The frequency then recovers partially, towards a value lower than the frequency measured before the earthquake. This suggests that the structure of IG-EPN was slightly damaged during the dynamic loading. The recovery immediately after the loading is similar with both of the monitoring methods, although differences remain for the short times, which affect the τ_{min} estimate.

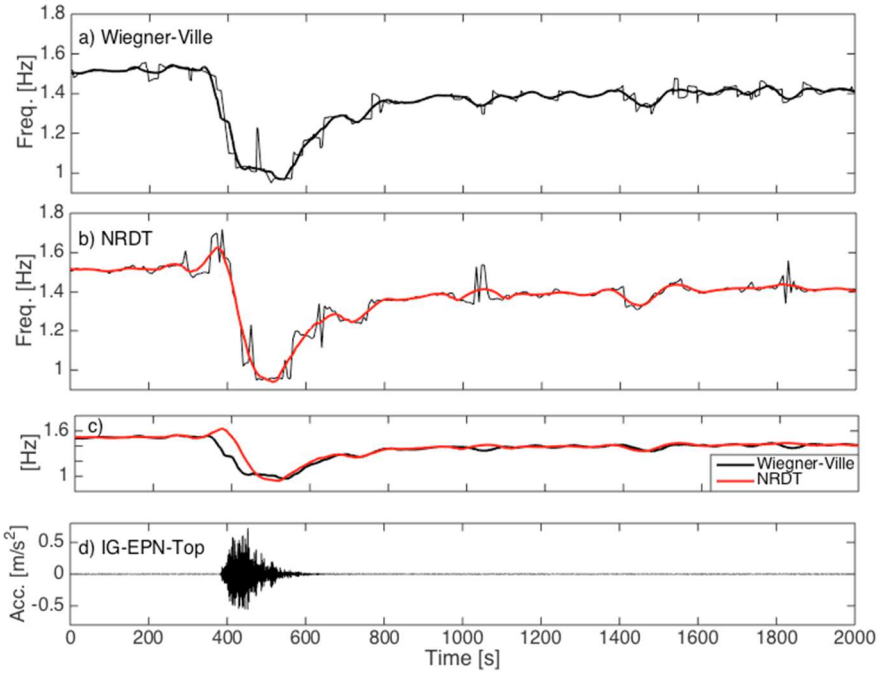

Figure 11. Monitoring of the resonance frequency at IG-EPN for the Pedernales earthquake. **(a)** WV and **(b)** NRDT. Thick lines, smoothed variations using a Savitzky-Golay fit function. **(c)** Smoothed function for NRDT and WV. **(d)** Time history of acceleration recorded at the top of IG-EPN.

The Snieder et al. (2016) model for characterising relaxation is shown as a function of the time logarithm in Figure 12 and Figure 13 for FB-UCLA and IG-EPN, respectively. The frequencies are normalised by their values at long times, as a convergence value of 1 is

required.

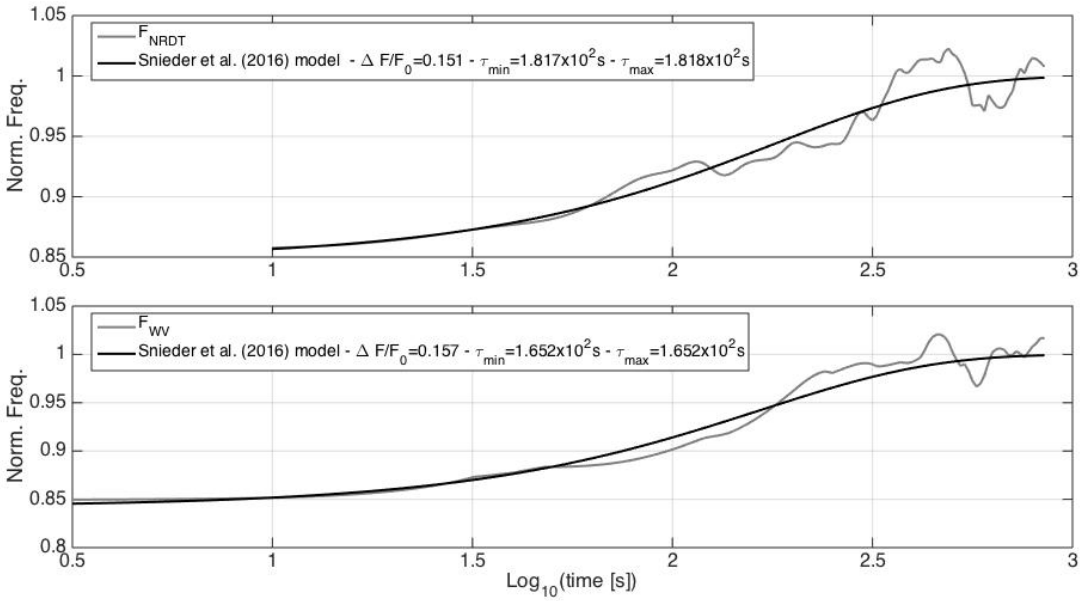

Figure 12. Recovery of the normalised frequency of the fundamental mode for FB-UCLA after the Chino Hills earthquake, using NRDT (upper panel) and WV (lower panel). Thick black line, Snieder et al. (2016) fit model; grey line, experimental smoothed normalised values of the fundamental frequency.

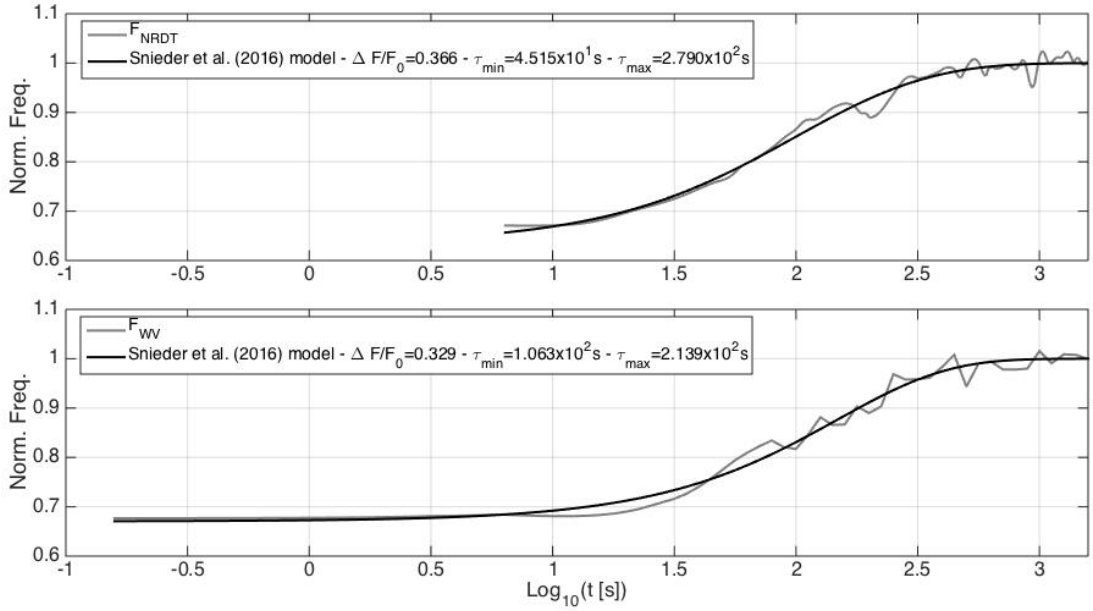

Figure 13. As for Figure 12 for IG-EPN for the Pedernales earthquake.

For FB-UCLA, the results obtained by NRDT and WV are comparable, with a co-seismic drop in frequency of around 0.15. τ_{min} and τ_{max} are very similar, at 182 s and 165 s for NRDT and WV, respectively. The minimum (τ_{min}) and maximum (τ_{max}) characteristic times are comparable, which according to the Snieder et al. (2016) model, suggests that the cracks or joints that are opened by the earthquake show a distribution of energy barriers, and therefore a distribution of characteristic sizes that is limited around a central value.

For IG-EPN, a few variations are seen, depending on the time–frequency monitoring

methods. The co-seismic frequency drop is around 33% to 36%. τ_{min} and τ_{max} are different, as 45 s to 106 s and 279 s and 214 s using NRDT and WV, respectively. The difference between the two monitoring methods indicates that in this specific case (Pedernales earthquake recorded at IG-EPN), the short characteristic times are not as well identified near the main shock, introducing uncertainties on the real state assessment of the building that must be considered before operational application. It is also interesting to note that the Pedernales shock was greater than the earthquake suffered by FB-UCLA, and it resulted in a permanent frequency variation after the main shock, which indicates increased cracking.

The conditioning sequence of IG-EPN also included a foreshock and an aftershock (Fig. 14a), with these two events generating transient frequency variations (Fig. 14b). Their amplitudes are smaller than that of the main shock, with the initial pre-loading recovered relatively quickly. The evolution of τ_{min} and τ_{max} with the damage is confirmed in Figure 15 and Table 2, which show the Snieder et al. (2016) function and the associated parameters applied to WV for the three events. The non-linearity measured increases as the deformation measured in the structure increases. $\Delta F/F_0$ is 0.087, 0.190 and 0.366 for the foreshock (deformation 16980 5.3 $\times 10^{-6}$), aftershock (1.7 $\times 10^{-5}$) and main shock (7.6 $\times 10^{-4}$), respectively. Furthermore, for the foreshock and aftershock, the two characteristic dimensions τ_{min} and τ_{max} are identical; i.e., 37 s and 66 s for the foreshock and aftershock, respectively. As mentioned previously for FB-UCL, this indicates that these moderate stresses only activate heterogeneities (i.e., cracks in the present case) the size distribution of which is limited around a main value. In such cases, the structure deformation is such that the existing cracks are stressed to their maximum, although no new cracks are formed. For the main shock, τ_{min} and τ_{max} are very different (45 s, 279 s, respectively), indicating the mobilising of new cracks created by a major deformation, as observed in the laboratory on the granite beam. τ_{max} is so much larger for the main shock than for the fore and after shocks because of the size of the cracks activated by this loading. The characteristic times τ_{min} also increase with each earthquake. According to the interpretation that links these times directly to crack size, the minimum size of the cracks opened by the successive stresses might increase as the dynamic loading events are repeated. In other words, the damage estimated after the permanent drop in frequency observed for the main shock consists, at least in part, in the lengthening of the crack sizes. Further analysis must be carried out on the accuracy and the values of τ_{min} and τ_{max} according to the amplitude of the loadings (or conditioning) and the weather condition.

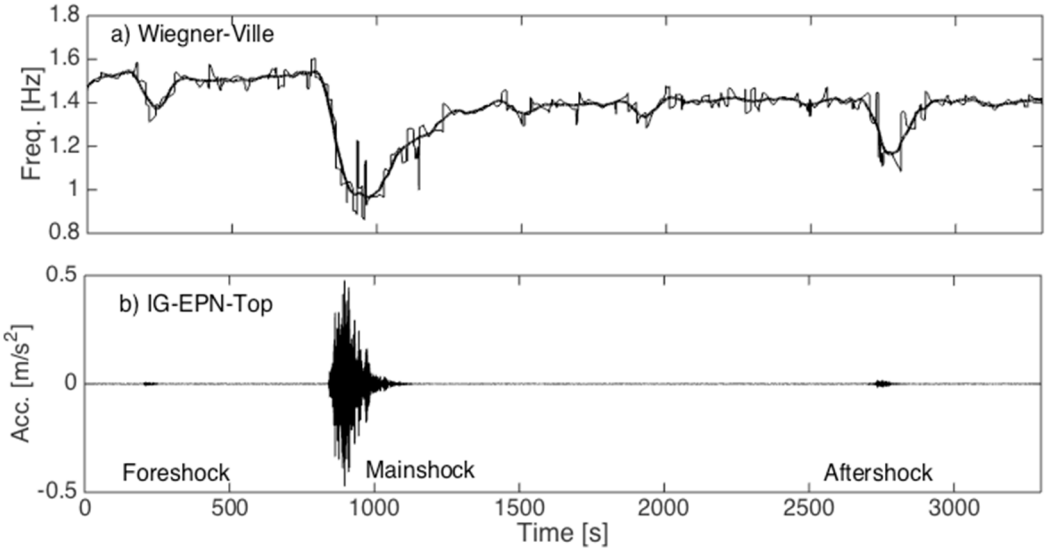

Figure 14. Fore-shock, main shock and after-shock earthquakes recorded for the IG-EPN building for the Pedernales sequence. **(a)** Wiegner-ville function applied to the variation of the resonance frequency (black) and the Savitzky-Golay smoothing function. **(b)** Time-history of acceleration at the top of IG-EPN.

Table 2. Parameters of the recovery relationships of the fundamental mode frequency of IG-EPN after the three events, as foreshock, main shock and aftershock, using the Snieder et al. (2016) model. Dmax is the maximal drift measured during each event by the relative displacement between the top and bottom, divided by the height.

Shock	$\left(\frac{\Delta F}{F_0}\right)$	$\tau_{min}(s)$	$\tau_{max}(s)$	D_{max}
Fore	0.087	37.22	37.24	5.3×10^{-6}
Main	0.366	45.15	279.0	7.6×10^{-4}
After	0.190	65.81	65.83	1.7×10^{-5}

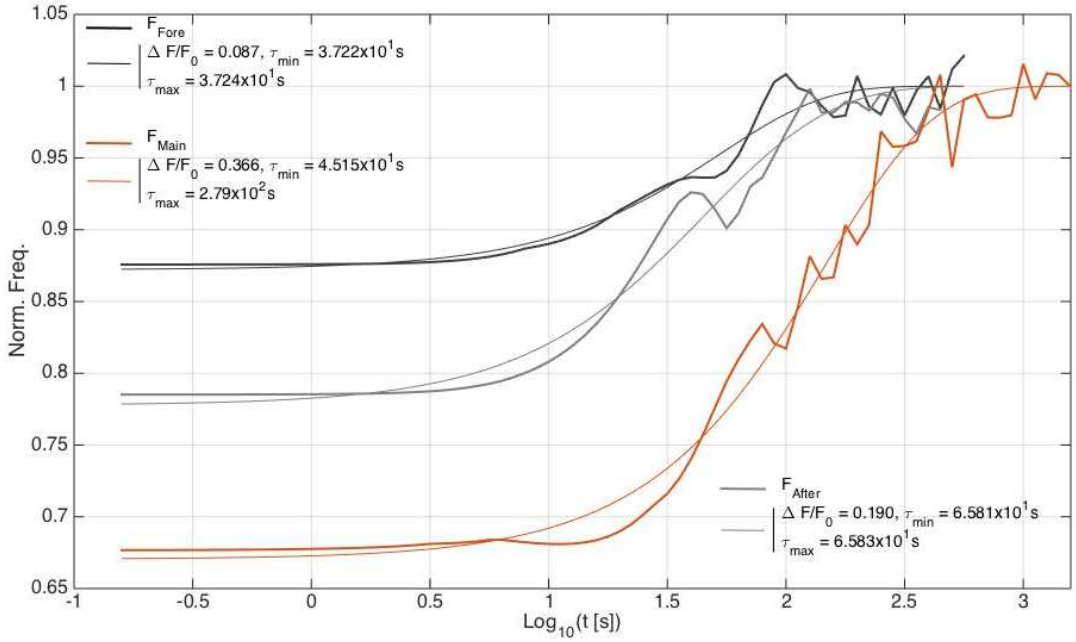

Figure 15. Recovery of the normalized frequency of the fundamental mode for IG-EPN for the fore-shock (black), the main shock (red) and the after-shock (grey) of the Pedernales sequence. Thick lines, experimental smoothed normalized values of fundamental frequency; continuous lines, *univ* fit models.

6. Conclusions

Analysis of the non-linear phenomena (i.e., ANFD, slow dynamics) observed in the granite beam before and after damage and in the actual civil engineering structures that suffered earthquakes confirm the direct relationship between the properties of elastic characteristic recovery (i.e., resonance frequency) and damage. This relationship between slow dynamics and the degree of system heterogeneity has already been confirmed at the laboratory scale and in seismology. For the first time, a detailed analysis of the slow dynamics applied to civil engineering structures is shown herein. It opens the route for monitoring the structural integrity of civil engineering structures. However, it is conditioned by the adjustment of the recovery model for system dynamics, and the possibility of precise monitoring of the various

elastic properties (or a proxy; i.e., resonance frequency, in the present case).

In this study, the two methods used are a modified version of a conventional method (NRDT), and a conventional method (WV). These showed differences for the characterisation of the short and long recovery times. At long times, as the recovery processes can be long (Astorga et al., 2018), it is also preferable to have continuous data, as for IG-EPN.

Using a laboratory analogue, i.e., the granite beam, recovery of the frequency fitted by a linear function of the time logarithm depends on the health state (i.e., damaged or undamaged) of the beam. In spite of the difficulties in adjusting the long and short characteristic times, the Snieder et al. (2016) model enabled the definition of a narrow correlation of characteristic times with damage. These data are fully confirmed in the civil engineering buildings, with the definition of the physical properties of the recovery according to the loading or damage, particularly for IG-EPN. Slow dynamics are observed after strong loadings, and for this level of strain (or structural drift), we assume little sensitivity to environmental conditions or conditioning, which suggests the absolute characterising of the damage.

We note that the characteristic times offer direct insights into the types of cracks. The designs of the buildings tested in the present study were different: FB-UCLA has a steel structure and IG-EPN has a reinforced concrete structure. The characteristics of the slow dynamics depend on both the deformation caused by the loading and the heterogeneities present in the structure. A drop in frequency was also observed in a unique building in Japan during a long series of seismic loading (Astorga et al., 2018). In that particular case, the frequency drop was conditioned by the deformation and damage that accumulated over time. For IG-EPN, the damage is also characterised by a faster recovery rate in the event of stronger loading. Without knowing their exact dimensions, the difference between τ_{min} and τ_{max} provides information on both the distribution of the energy barriers, and therefore the cracks, and on their evolution according to the level of loading.

We have shown that the characteristic times τ_{min} and τ_{max} were very close, both for FB-UCLA and its moderate earthquake (Chino Hills), and for IG-EPN for the foreshock and the aftershock. This indicates a limited distribution around a central value of the sizes of the cracks opened by the seismic event, without the creation of new cracks. In the case of FB-UCLA, which mainly constituted a steel structure, the structural elements are not fractured, and the time constants correspond to the energy barriers associated with the joints between the structural elements. IG-EPN is made of reinforced concrete, which is known to fracture. The proximity of τ_{min} and τ_{max} suggests that only the smallest cracks were opened by the two low amplitude earthquakes. In the case of IG-EPN, the increase in τ_{min} with the deformation caused by the earthquakes also indicates increased cracking caused by the seismic damage. This increase is confirmed by the difference between τ_{min} and τ_{max} observed during the main shock, and similarly between the undamaged and damaged beams. This observation enables us to envisage a data-driven method for monitoring structure integrity in the event of seismic loadings in a sequence. This is all the more important as damage affects the response, and therefore the vulnerability, of structures (Iervolino et al., 2014; Trevlopoulos and Guéguen, 2017), with probable consequences on the safety of the local inhabitants in the event of a seismic crisis.

The sensitivity and accuracy of τ_{min} and τ_{max} with damage, and according to the conditioning and the weather condition, must be investigated before concluding on a possible operational framework for structural monitoring. The sensitivity of the resonance frequency and of its recovery to weak loadings may control the efficiency of this model for monitoring and must also be considered before operational application. In addition, adjustment of the Snieder et al. (2016) relaxation model via a non-linear regression algorithm is difficult to implement. There are other models, and although these have only been applied in a laboratory

setting to date (Shokouhi et al., 2017), if applied to civil engineering structures (Astorga et al., 2019), these could provide more precise information on the nature of the cracks (i.e., dimension, energy, distribution), including sensitivity to the conditioning and the external forcing such as temperature or humidity.

Acknowledgment

This contribution is part of an Ecuadorian-French cooperation program between the Instituto Geofisico, Escuela Politécnica Nacional (IGEPN), Quito, Ecuador, and the Institut de Recherche pour le Développement (LMI SVAN). This work is supported by the French project REMAKE (Seismic Risk in Ecuador: Mitigation, Anticipation, and Knowledge of Earthquakes, ANR-15-CE04-0004) and by both Ecuadorian projects SENPLADES (Generación de capacidades para la difusión de alertas tempranas y para el desarrollo de instrumentos de decisión ante las amenazas sísmicas y volcánicas dirigidos al Sistema nacional de gestión de riesgos) and SENESCYT (Intituto Geofisico-EPN: Ampliacion y Modernizacion el servicio nacional de sismologia y vulcanologia). The Factor Building instrumentation was funded by USGS and data were downloaded from www.iris.edu. This study is part of the Urban Seismology project of the Earth Sciences Institute (Université Grenoble Alpes), and was supported by funding from Labex OSUG@2020 (Investissements d'avenir, ANR10-LABX56). M-A Brossault was funded by the Auvergne-Rhône-Alpes Region.

References

Asmussen JC. Modal analysis based on the random decrement technique: application to civil engineering structures. *Doctoral dissertation University of Aalbord* 1997.

Astorga A.L., Guéguen P., Riviere J., Kashima T., Johnson, P.A. Recovery of the resonance frequency of buildings following strong seismic deformation as a proxy for structural health. *Structural Health Monitoring*, 2019. https://doi.org/10.1177/1475921718820770

Astorga A.L., Guéguen P., Rivière J., Kashima T. Johnson P.A. Recovery of the resonance frequency of buildings following strong seismic deformation as a proxy for structural health. Structural Health Monitoring, 2019. doi:10.1177/1475921718820770

Bocquet L, Charlaix E, Ciliberto S, Crassous J. Moisture-induced ageing in granular media and the kinetics of capillary condensation. *Nature* 1998;396(6713):735.

Boutin C, Hans S, Ibraim E, Roussillon P. In situ experiments and seismic analysis of existing buildings. Part II: Seismic integrity threshold. *Earthquake Engineering & Structural Dynamics* 2005;34(12):1531-1546.

Brenguier F, Campillo M, Hadziioannou C, Shapiro NM, Nadeau RM, Larose E. Postseismic relaxation along the San Andreas fault at Parkfield from continuous seismological observations. *Science* 2008;321(5895):1478-1481.

Brossault MA, Roux P, Guéguen P. The fluctuation–dissipation theorem used as a proxy for damping variations in real engineering structures. *Engineering Structures*, 2018;167:65-73.

728 Chernis PJ, Robertson PB. *Thermal cracking in Lac du Bonnet granite during slow heating to*
729 *205 degrees celsius* (No. AECL--10937). Atomic Energy of Canada Ltd., 1993.

730 Clinton JF, Bradford SC, Heaton TH, Favela J. The observed wander of the natural
731 frequencies in a structure. *Bulletin of the Seismological Society of America* 2006;96:237-257

732 Cole HA. *On-the-line analysis of random vibrations.* AIAA Paper 1968;No. 68-288.

733 Guéguen P, Hamze A, Baillet L, Roux P. Numerical and experimental assessment of the
734 performance of four nondestructive damage evaluation methods in situations comparable to
735 post-earthquake damage analysis. *International Journal of Earthquake Engineering. Special*
736 *Issue: Structural Health Monitoring*. 2014

737 Guéguen P, Johnson P, Roux P. Nonlinear dynamics induced in a structure by seismic and
738 environmental loading. *The Journal of the Acoustical Society of America* 2016*;140*(1):582-
739 590.

740 Guyer RA, McCall KR, Boitnott, GN. Hysteresis, discrete memory, and nonlinear wave
741 propagation in rock: A new paradigm. *Physical review letters* 1995;74(17):3491.

742 Guyer RA, Johnson PA. Nonlinear mesoscopic elasticity: Evidence for a new class of
743 materials. *Physics today* 1999;52:30-36.

744 Iervolino I, Giorgio M, Chioccarelli E. Closed-form aftershock reliability of damage-
745 cumulating elastic–perfectly-plastic systems. *Earthq Eng Struct Dyn* 2014;43:613–25.

746 Johnson PA, Zinszner B, Rasolofosaon PNJ. Resonance and elastic nonlinear phenomena in
747 rock. *Journal of Geophysical Research: Solid Earth* 1996;101.B5:11553-11564.

748 Johnson PA, Sutin A. Slow dynamics and anomalous nonlinear fast dynamics in diverse
749 solids. *The Journal of the Acoustical Society of America* 2005;117(1):124-130.

750 Kohler MD, Davis PM, Safak E. Earthquake and ambient vibration monitoring of the steel-
751 frame UCLA Factor building. *Earthquake Spectra* 2005;21(3):715-736.

752 Larose E, Tremblay N, Payan C, Garnier V, Rossetto V. Ultrasonic slow dynamics to probe
753 concrete aging and damage. In *AIP Conference Proceedings* 2013; 1511(1): 1317-1324.

754 Lott M, Remillieux MC, Garnier V, Le Bas P-Y, Ulrich TJ, Payan C. Nonlinear elasticity in
755 rocks: A comprehensive three-dimensional description. *Physical Review Materials* 2017;1(2):
756 023603.

757 Lott M, Payan C, Garnier V, Le Bas P-Y, Ulrich T J, Remillieux MC. Three-dimensional
758 modeling and numerical predictions of multimodal nonlinear behavior in damaged concrete
759 blocks. *The Journal of the Acoustical Society of America* 2018;144(3):1154-1159.

760 Mikael A, Guéguen P, Bard PY, Roux P, Langlais M. The analysis of long-term frequency
761 and damping wandering in buildings using the Random Decrement Technique. *Bulletin of the*
762 *Seismological Society of America* 2013;103:236-246. Doi:10.1785/0120120048

763 Michel C, Guéguen P. Time-frequency analysis of small frequency variations in civil
764 engineering structures under weak and strong motions using a reassignment method. *Struct.*
765 *Health Monit* 2010;9(2):159-171.

766 Michel C, Guéguen P. Interpretation of the velocity measured in buildings by seismic
767 interferometry based on Timoshenko beam theory under weak and moderate motion. *Soil*
768 *Dynamics and Earthquake Engineering* 2018;104:131-142.

769 Nasser F, Li Z, Martin N, Guéguen P. An automatic approach towards modal parameter
770 estimation for high-rise buildings of multicomponent signals under ambient excitations via
771 filter-free Random Decrement Technique. *Mechanical Systems and Signal Processing*
772 2016;70:821-831.

773 Nayeri RD, Masri SF, Ghanem RG, Nigbor RL. A novel approach for the structural
774 identification and monitoring of a full-scale 17-story building based on ambient vibration
775 measurements. *Smart Materials and Structures* 2008;17(2):025006.

776 Orfanidis, SJ. *Introduction to signal processing*. Prentice-Hall, Inc., 1995.

777 Peng Z, Ben-Zion Y. Temporal changes of shallow seismic velocity around the Karadere-
778 Düzce branch of the north Anatolian fault and strong ground motion. *Pure and Applied*
779 *Geophysics* 2006;163(2-3):567-600.

780 Perrault M, Guéguen P, Aldea A, Demetriu S. Using experimental data to reduce the single-
781 building sigma of fragility curves: case study of the BRD tower in Bucharest, Romania.
782 *Earthquake Engineering and Engineering Vibration* 2013;12(4):643-658.

783 Roux P, Guéguen P, Baillet L, Hamze A. Structural-change localization and monitoring
784 through a perturbation-based inverse problem. *The Journal of the Acoustical Society of*
785 *America* 2014;136(5):2586-2597.

786 Scalerandi M, Bentahar M, Mechri C. Conditioning and elastic nonlinearity in concrete:
787 Separation of damping and phase contributions. *Construction and Building Materials*
788 2018;161:208-220.

789 Shokouhi P, Rivière J, Lake CR, Le Bas PY, Ulrich TJ. Dynamic acousto-elastic testing of
790 concrete with a coda-wave probe:comparison with standard linear and nonlinear ultrasonic
791 techniques. *Ultrasonics* 2017;81:59-65.

792 Skolnik D, Lei Y, Yu E, Wallace JW. Identification, model updating, and response prediction
793 of an instrumented 15-story steel-frame building. *Earthquake Spectra* 2006;22(3):781-802.

794 Snieder R, Sens-Schönfelder C, Wu R. The time dependence of rock healing as a universal
795 relaxation process, a tutorial. *Geophysical Journal International* 2016;208(1):1-9.

796 Takarli M, Prince-Agbodjan W. Temperature effects on physical properties and mechanical
797 behavior of granite: experimental investigation of material damage. *Journal of ASTM*
798 *International* 2008;5(3):1-13.

799 TenCate JA, Smith E, Guyer RA. Universal slow dynamics in granular solids. *Physical*
800 *Review Letters* 2000;85(5):1020.

801 Trevlopoulos K, Guéguen P. Period elongation-based framework for operative assessment of
802 the variation of seismic vulnerability of reinforced concrete buildings during aftershock
803 sequences. *Soil Dynamics and Earthquake Engineering* 2016;84:224-237.

804 Wu C, Peng Z, Ben-Zion Y. Non-linearity and temporal changes of fault zone site response
805 associated with strong ground motion. *Geophysical Journal International* 2009;176(1):265-
806 278.

807 Zhang, H., Li H-N, Li C, Cao G-W. Experimental and numerical investigations on seismic
808 responses of reinforced concrete structures considering strain rate effect. *Construction and*
809 *Building Materials* 2018; 173(10):672-686.